between smooth plains and the surrounding terrain indicating compositional differences. In at least two cases the smooth plains overlie material that is bluer (higher UV/orange ratio) and is enriched in opaque minerals relative to the hemispheric average. Since the smooth plains are probably old lava flows (see Chapter 10), and the FeO solid/liquid *distribution coefficient* is about 1% during partial melting, it is estimated that the Mercury's mantle has a FeO abundance similar to the lava flows (less than 3%). But this is very sensitive to the degree of partial melting.

8.5 SUMMARY

Both Earth-based spectroscopic observations and calibrated *Mariner 10* images indicate that the surface of Mercury is heterogeneous in composition with a wide range of SiO_2 content. The FeO content appears to be between 1 and 3% which is abnormally low compared to other terrestrial planets and the Moon. Evidence for pyroxene appears to be of the Mg-rich or Ca-rich type. The spectroscopic data are consistent with compositions ranging from low-iron basalts and anorthosites. There are also spectra that exhibit similarities to laboratory spectra of *syenite*. However, to have a rock so highly evolved petrologically requires multiple episodes of partial melting which may be problematical for Mercury.

Photometry of Mercury's surface in the UV and visible indicates Mercury is fairly smooth, consistent with flooding by lavas. The morphology of the land forms, which will be discussed in detail later in Chapter 10, indicate fluid lava flows over much of the surface. *Mariner 10* imaging ratios indicate bright excavated regions. Ground-based spectroscopy indicates that these excavated regions may be anorthosites. This would be consistent with the appearance of enhanced regions of Na atmosphere that are associated with the fresh craters as discussed in Chapter 6. Continued ground-based observations and detailed measurements by *MESSENGER* should greatly expand our knowledge of the variety of compositions and their spatial distribution.

9

The impact cratering record

9.1 MERCURY'S MOST COMMON LANDFORM

Mercury is one of the most heavily cratered planets in the Solar System, and its cratering record provides important information on the cratering process and crater characteristics in that part of the Solar System. Because Mercury is the innermost planet, it provides important constraints on the origin of impacting objects in the terrestrial planet domain.

9.1.1 It all began with the Moon

In 1609 Galileo recognized and wrote about craters he viewed with the recently invented telescope. The craters he saw, were common on the Moon. In fact, the most common landforms in the Solar System are impact craters. They occur in greater or lesser abundance on almost all solid bodies explored to date.

9.1.2 Three basic crater characteristics

There are three basic characteristics common to all relatively fresh impact craters:

(1) a near-circular raised rim;
(2) a floor that is deeper than the crater surroundings; and
(3) a relatively rough *ejecta blanket* that surrounds the crater.

Small craters have bowl-shaped interiors and are called simple craters. Larger craters have terraced inner walls, a relatively flat floor, *central peaks* and are called complex craters. The rim structure consists of a flap of overturned material resulting in inverted *stratigraphy* (older on top and younger on the bottom). The crater is surrounded by an extensive ejecta deposit consisting of two parts: a relatively narrow inner zone of continuous hummocky ejecta; and an outer zone consisting of strings and clusters of secondary craters caused by the impact of discrete masses of ejecta. Fresh craters have ray systems consisting of newly excavated material associated with secondary craters.

On Mercury, impact craters are found on all types of terrain and in various states of preservation. They are the dominant landform on the planet. The largest relatively well preserved impact feature seen by *Mariner 10* is the 1300 km diameter Caloris basin. Probably craters less than a millimeter in diameter have formed from dust-sized micrometeorites, based on *Apollo* lunar returned samples. Some craters are fresh with extensive *ray systems* while others are so degraded that only discontinuous remnants of their rims remain. It is believed that the two large radar anomalies (A and B) on Mercury's unseen side are relatively recent impact craters (see Chapter 7).

9.2 CRATER FORMATION

9.2.1 Energy of impact

When high velocity objects strike planetary surfaces they produce enormous amounts of kinetic energy. The amount of energy produced is $\frac{1}{2}mv^2$ where m is the mass of the object and v is its impact velocity. For example, if a 1-km diameter iron meteorite hit the Earth at 15 km/s it would release an amount of energy equivalent to about 100,000 megatons of TNT (1 megaton is 1 million tons). That amount of energy would produce a crater about 12 km in diameter.

9.2.2 Crater diameter and depth

The diameter of impact craters depends on a number of parameters besides velocity and mass. Among these are the size of the projectile, the ratio of projectile to surface density, surface gravity, impact angle, and for larger *complex craters*, the transition diameter from simple to complex craters. Because Mercury is so close to the Sun, the large gravitational pull of the Sun causes objects to impact Mercury at velocities greater than all other planets for given projectile orbital characteristics. For instance, on average, asteroids will impact Mercury at a velocity of about 34 km/s, compared to 22 km/s on the Moon and 19 km/s on Mars. Parabolic comet impacts (comets from the outer fringe of the Solar System) should be much more frequent on Mercury than other bodies (about 41% of the craters on Mercury, about 10% on the Moon and Earth, and less than 3% on Mars). On Mercury, comet impacts will have an average velocity of about 87 km/s compared to 52 km/s on the Moon and 42 km/s on Mars. Therefore, craters will generally be larger and produce more melt and ejecta on Mercury than on other planets and satellites for similar sized objects with similar physical characteristics.

In an impact event, kinetic energy is rapidly transferred to the planetary crust. Most of the energy takes the from of shock waves that travel at supersonic speeds through both the crust and the impacting object. They spread out in a hemispherical shell from the point of impact. As the shock waves pass through the rocks they are

subjected to very high pressures that can rise to hundreds of kilobars (kbar). Granite is crushed at 250 kbar, melted at about 450 kbar and vaporized at 600 kbar. It is the interaction of the shock waves with the unconfined surface that excavates the crater. As the shock wave passes through the compressed rocks they snap back along the unconfined surface. This produces what is called a tensional *rarefaction wave* that decompresses and fractures the rock. The net effect is to momentarily convert the rock to a fluid-like material that moves laterally upward and out of a steadily growing excavation cavity. The cone of rapidly moving ejecta is mainly deposited beyond the crater's final rim. The crater stops growing when the strength of the target material exceeds the decaying strength of the shock wave. This initial crater is called the excavation crater, but may be enlarged by slumping of the rim into the crater if the crater is large enough. The rock layers at the edge of the crater are pushed upward and overturned by the passage of the shock wave to produce the characteristic raised rim of impact craters. Of course, well before this time the projectile has been completely destroyed as the shock waves generated in the projectile interact with the unconfined surface. It essentially explodes, some of it vaporized, some melted, and the rest shattered into small pieces. It is possible to see many of these features of impact craters on Earth, for example, at Meteor crater near Winslow, Arizona. It was formed when an iron meteorite estimated to have been about 30 m in diameter and with a mass of about 100,000 tons excavated a crater about 1.2 km in diameter. The eroded rim rises about 47 m above the surrounding topography, and 174 m above the crater floor.

9.2.3 Volatilization and melting of surface and impactor

Not all the kinetic energy of the impactor is used to excavate the crater. Some is partitioned into heat. The heat can be so great that a large volume of the target material is melted and volatilized. In large craters impact melt is found as a sheet overlying fragmented floor material, as ponds and flows on the crater rim, and as part of the continuous ejecta blanket. Great plumes of atoms and molecules may be sent far above the surface and contribute to a temporary atmosphere.

As discussed in Chapter 6, much of the Na, K, and Ca atmosphere observed from ground-based spectroscopy is created in the volatilization following impact of interplanetary dust particles on Mercury's surface.

9.3 CRATER MORPHOLOGY

9.3.1 Three general crater morphologies

The morphology of Mercurian craters is similar to that of lunar craters in most respects. Like the Moon, the general structure of Mercurian impact craters can be divided into three types (Figure 9.1). At diameters less than 10 km they have bowl-shaped profiles with raised rims. At diameters greater than 10 km they have central peaks, flat floors and terraced inner walls. Therefore, on Mercury the transition

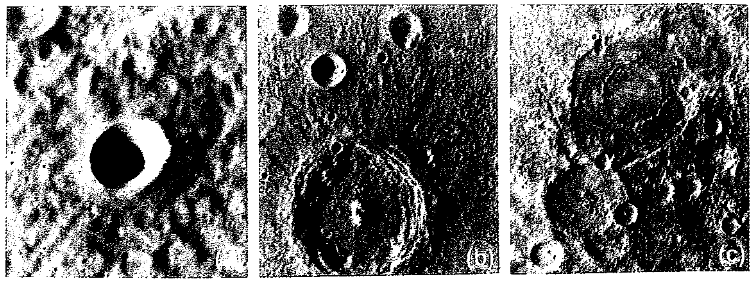

Figure 9.1. Three Mercurian craters show the change in morphology with increasing size. In (a) the crater is 8 km diameter and has a bowl-shaped depression. At diameters between 15 and 100 km the craters have central peaks and terraces on the interior rims. The crater Brahms in the center (b) is a complex crater 75 km diameter. At diameters greater than 100 km craters develop central rings as shown by the 225 km Bach basin (c).

diameter from simple to complex craters occurs at 10 km. The transition diameter is not the same on all bodies. On the Moon it occurs at 19 km and on Earth it is about 3 km. The transition diameter depends primarily on the surface gravity; the stronger the surface gravity the smaller the transition diameter. Although gravity seems to be the most important factor controlling the transition diameter, the physical characteristics of the target material are also important. For example, on Earth the transition diameter is smaller in weaker sedimentary rocks than in stronger crystalline rocks. On Mars the transition diameter is smaller than on Mercury (5 compared to 10 km) although their surface gravities are the same. This has been used as evidence for a weaker ice/water-rich layer on Mars.

In small *simple craters* there is little or no inward slumping of the rim, and the final crater is essentially the excavation crater. In complex craters the excavation crater is enlarged by inward slumping of the rim. With large craters between 15 to 200 km diameter rim slumping can enlarge the crater considerably. At very large diameters associated with impact basins, whole sections of the crust collapse into the excavation cavity to enlarge the diameter by tens to hundreds of kms.

At the largest diameters the craters show double or multiple rings (Figure 9.1(c)). At these sizes they are usually referred to as impact basins. On Mercury double ring basins begin to form at about 200 km diameter and multiple rings at about 750 km diameter. At the lower diameters of double ring basins, central peaks are usually present. The morphology of these impact basins will be discussed in more detail in Section 9.5.

9.3.2 Difference in Physical Properties of Lunar and Mercurian Highlands

There are significant differences in the abundances of central peaks, terraces, and scalloped crater rims between fresh craters in the lunar maria and highlands

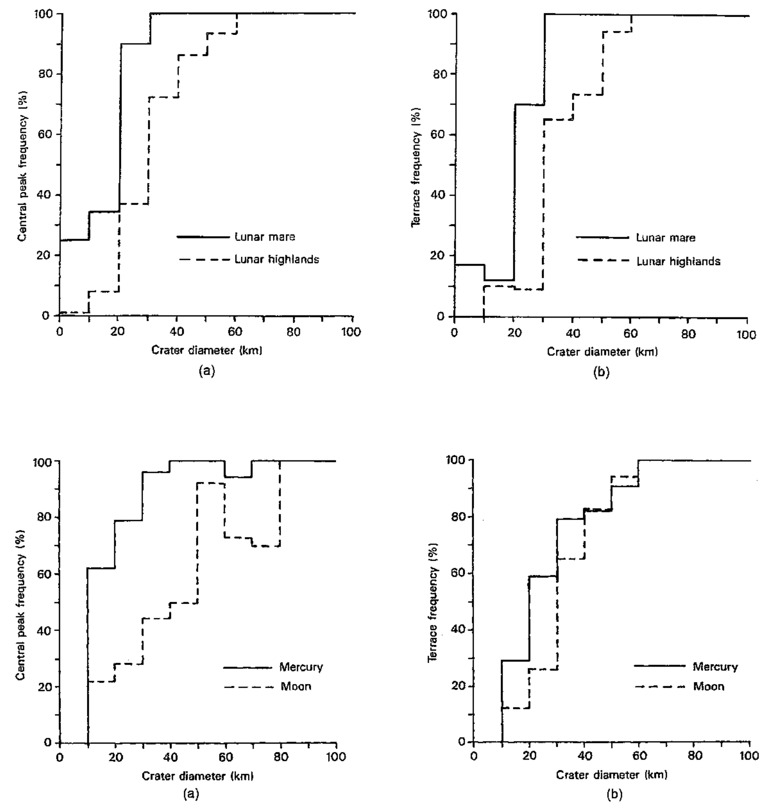

Figure 9.2. Histogram of the central peak (a) and terrace (b) frequency versus crater diameter for the lunar highlands and maria (top). Histogram of the central peak (a) and terrace (b) frequency versus crater diameter for the Moon and Mercury (bottom) (from Smith and Hartnell, 1979).

(Figures 9.2 and 9.3). This has been attributed to differences in the physical properties of the lunar highlands and maria. The highlands is composed of a thick regolith and breccia (the *megaregolith*), and the maria consist of a thin regolith underlain by relatively unbrecciated volcanic lava flows. Furthermore, the morphologies of craters formed in the lunar maria, the Mercurian smooth plains, and the Mercurian highland cratered terrain are similar. However, there are large differences between the crater morphologies in the lunar highlands and the analogous Mercurian

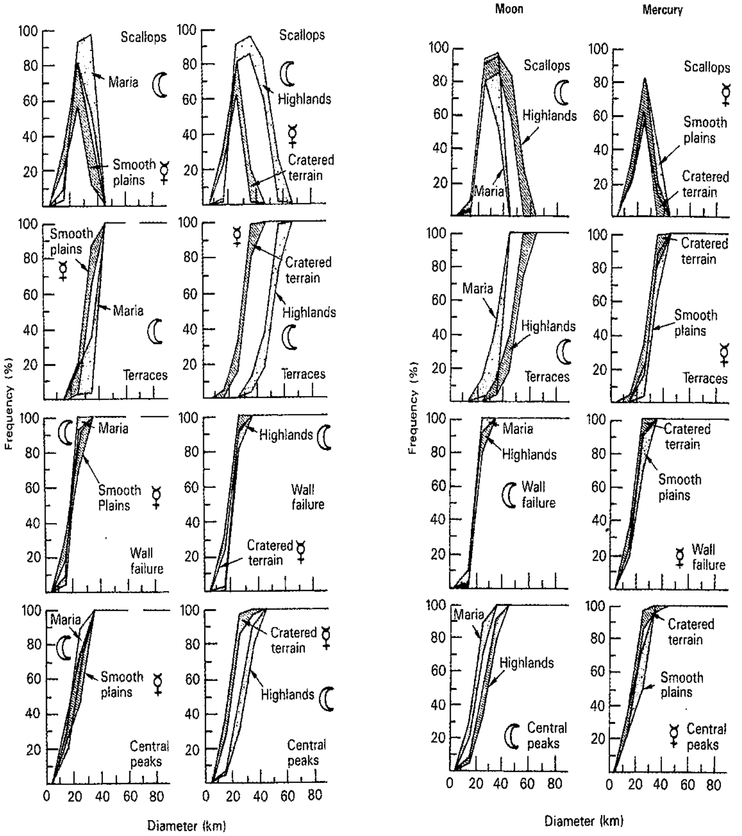

Figure 9.3. The first two columns of plots show the morphology/frequency distribution comparing craters on the lunar Maria to those in the Mercurian smooth plains (first column on left), and craters in the lunar highlands to those in the Mercurian cratered terrain (second column on left). The third and fourth columns are plots showing the morphology/frequency distribution, illustrated as ±1 sigma envelopes around the mean values, for craters on the Moon (third column) and Mercury (fourth column) (from Cintala *et al.*, 1977).

cratered highlands (Figure 9.3). This suggests that a difference in the physical properties of the target material, rather than surface gravity, is the major factor affecting interior crater morphology. The main difference between the lunar and Mercurian highlands is the great abundance of intercrater plains in the Mercurian highlands

(see Chapter 10). The lunar highlands have only small patches of intercrater plains that can be identified as ejecta deposits from certain basins (see Figure 9.21). These differences suggest that the Mercurian intercrater plains consist of a more coherent, stronger material akin to solid rock, rather than the less coherent, weaker megabreccia of the lunar highlands.

9.4 EJECTA DEPOSITS

9.4.1 Two distinct regions of crater ejecta

Impact crater ejecta consists of two parts:

(1) a continuous ejecta blanket; and
(2) discontinuous ejecta beyond the continuous ejecta.

The continuous ejecta consists of a blanket of hummocky ejecta extending about 0.5 to 1 crater diameter from the crater rim. The area covered by the blanket can be four to nine times the area of the crater. Discontinuous ejecta consists of swarms of secondary impact craters formed by clots, strings, or individual fragments thrown beyond the continuous ejecta blanket. Individual fragments can be thrown for hundreds or thousands of kilometers. Very fresh craters have bright ray systems that consist of secondary craters having their own ejecta deposits consisting of fresh, bright material. Powdery material created by the impact also contributes to the rays. Ejecta can have far-reaching effects on planetary and satellite surfaces. If fragments are ejected at velocities exceeding the escape velocity of the planet or satellite, they will not return to the surface. In fact, we have samples of Mars and the Moon here on Earth that were ejected at velocities greater than the escape velocities of the parent bodies.

Ejected particles travel on looping paths called ballistic trajectories. For airless bodies like the Moon and Mercury, the distance a fragment will travel depends on the velocity and angle at which it is ejected and the gravity field of the planet. Most ejecta material is ejected at angles between 30° and 50° from the horizontal. For any given ejection velocity, a fragment will travel farther when ejected at an angle of 45° (Figure 9.4). Another parameter that effects the distance traveled is the radius of curvature of the planet or satellite: the smaller the radius of curvature the greater the distance traveled. On bodies with an atmosphere like the Earth and Venus, atmospheric drag will reduce the distance ejecta can travel.

9.4.2 Ejecta differences between Mercury and the Moon

The characteristics of Mercurian ejecta deposits are different from those on the Moon. On Mercury the continuous ejecta deposits and secondary impact craters are closer to the crater rim than similar sized craters on the Moon. This is the result of the greater surface gravity on Mercury (370 cm/sec^2) than on the Moon (162 cm/sec^2); for a given ejection velocity objects will travel about half the distance on Mercury. Thus the continuous ejecta blanket only extends outward to about

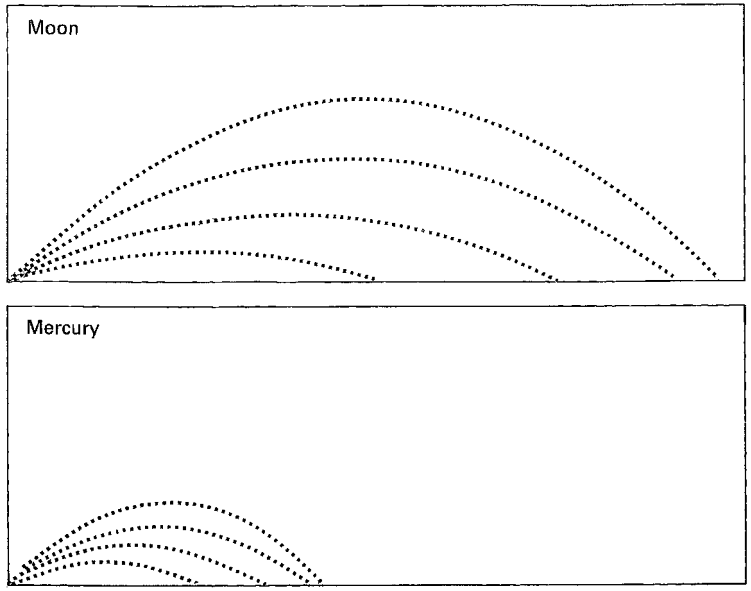

Figure 9.4. Diagram showing the ballistic trajectories for ejecta on the Moon and Mercury for the same impact conditions. Because of Mercury's much stronger gravity field, ejecta will travel more than twice as far on the Moon than on Mercury (from Strom, 1987).

0.5 crater radius. Also individual fragments travel shorter distances on Mercury than the Moon. On Mercury strings of secondaries often occur on the continuous ejecta blanket very close to the rim. This is rarely the case on the Moon. Thus, on Mercury both the continuous ejecta deposit and a greater abundance of secondary craters are concentrated nearer the crater rim (Figures 9.5 and 9.6). One apparent contradiction to this is the observation that some fresh craters have individual rays that extend enormous distances: much greater than fresh lunar craters of comparable size. Possibly these craters were formed by parabolic comets whose impact velocity at Mercury is exceedingly high (see section 9.2 on impact velocities on Mercury). In these cases possibly the ejection velocity of some swarms of fragments was extremely high and made up for the greater gravity field.

9.4.3 Crater degradation

The formation of impact craters and their ejecta deposits takes only seconds to minutes depending on the size of the impact. Over time, however, craters are

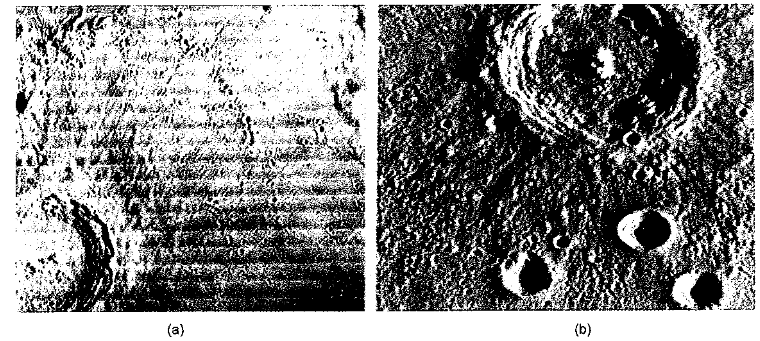

Figure 9.5. Comparison of the ejecta deposits for the lunar crater Copernicus (a) and a similar sized Mercurian crater (b). The ejecta deposit on the Mercurian crater is closer to the rim because of the higher gravity.

modified by a variety of processes. On Mercury, craters have been modified by three processes:

(1) subsequent impacts by both large and small objects including ejecta;
(2) volcanic deposition; and
(3) tectonic deformation.

Subsequent impacts have destroyed portions of pre-existing rims and ejecta blankets have obscured crater structures. Volcanic flooding has obliterated ejecta blankets or partially buried craters, and tectonic deformation has shifted the rims or floors and distorted the shape of craters. These processes have resulted in various degrees of crater degradation from slightly modified rims and ejecta deposits to barely discernable discontinuous rims (Figure 9.7).

9.5 THE CALORIS AND OTHER IMPACT BASINS

Very large impacts that form basins are devastating events for a planet or satellite. Their effects are so widespread that few areas of the planet are unaffected. Large impacts can trigger internal events that affect large areas of the planet. About 16 multiple ring basins larger than about 250 km diameter have been recognized on the 45 percent of Mercury observed by *Mariner 10*. About 15 impact basins have been located on the entire Moon. The largest basin so far seen on Mercury is the 1,560 km Borealis basin located near the north pole. This basin is very old and has been severely degraded. It is filled with smooth plains that embay and partially cover older craters. Much of the 45 percent of the planet was seen at high sun angles where it is difficult to discern structures, so it is possible that other basins occur in this 45 percent of the planet.

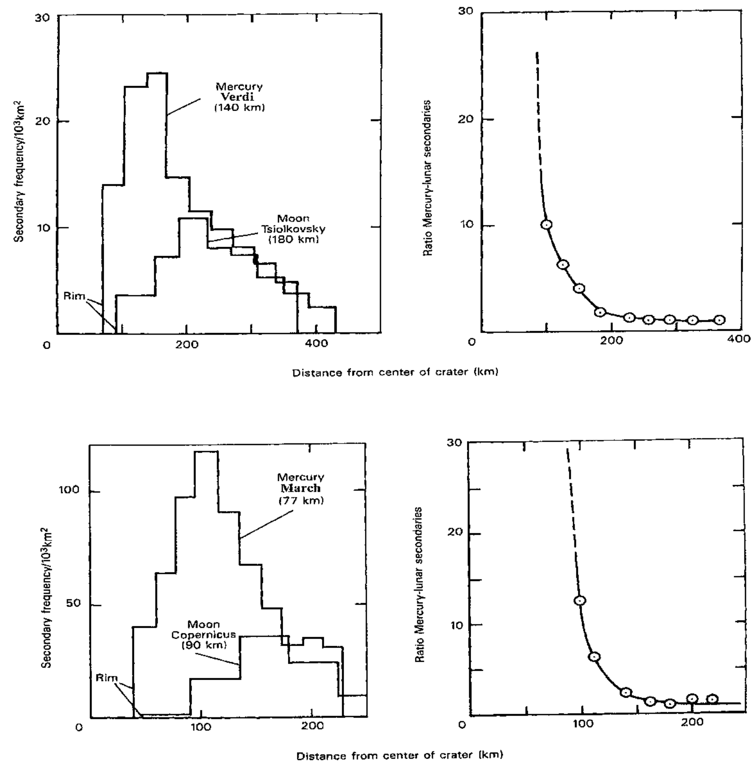

Figure 9.6. Plot of the radial variations in the areal density of secondary craters and the ratios of Mercurian to lunar secondary craters for the Mercurian craters Verdi and March and for the lunar craters Copernicus and Tsiolkovsky (from Gault *et al.*, 1975).

On Mercury the inner rings of the basin are often low, partial, or discontinuous, and, therefore, more inconspicuous than those on the Moon. Unlike the Moon, basins commonly have a partial, weak ring exterior to the main ring. The radial spacing of interior rings increases incrementally outward by about $\sqrt{2}$ of the diameter.

The basin topography and transient cavity size of Beethoven basin has been compared with lunar and Martian basins in conjunction with gravity data on those bodies, to infer the crustal viscosity at the time of impact. This comparison suggests that the crustal viscosity of Mercury during the period of heavy bombardment was relatively high, possibly due to an extremely dry crust.

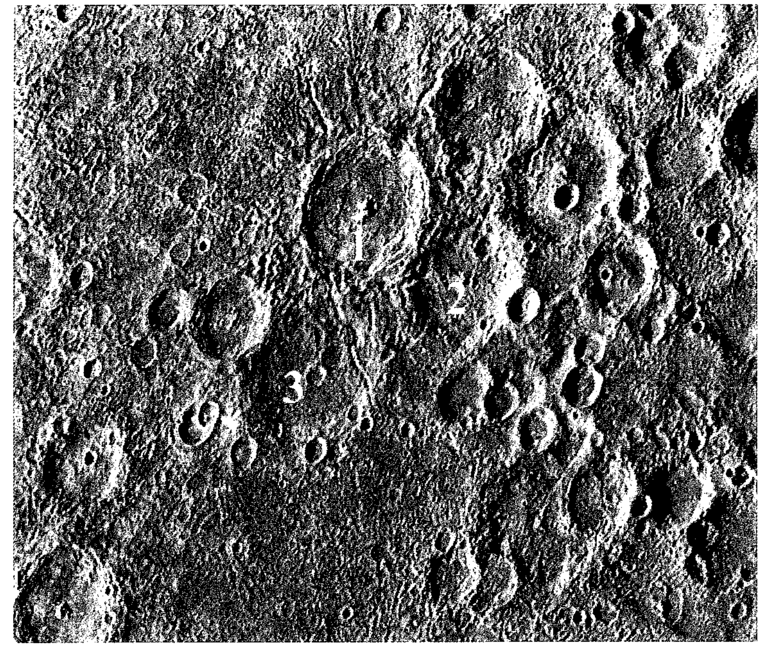

Figure 9.7. This image in the heavily cratered highlands of Mercury shows the various degradational stages of craters. Crater 1 is the freshest crater with a sharp rim and prominent ejecta deposits, while crater 2 has been degraded by subsequent cratering and the ejecta deposit of crater 1. Crater 3 is even more degraded by subsequent impacts, secondary cratering, and the flooding of its southern rim by intercrater plains material.

The largest, best preserved impact feature observed by *Mariner 10* is the Caloris basin (Figure 9.8). It is 1300 km in diameter and was observed half-lit at the terminator. Its formation affected large areas surrounding the basin and also caused a tremendous amount of fracturing and surface disruption at the Caloris antipode; 180° away on the opposite hemisphere of the planet (to be discussed in detail in Section 9.6). The number of rings ranges from 3 to perhaps 6. The main ring of mountains is about 2 km high. Another faint cliff is located on the northeastern rim about 150 km from the main rim (Figure 9.9). It probably represents a fault scarp along which a block of the crust slid inward toward the excavation crater. The area between the scarp and the main rim consists of broken up material probably formed as blocks slid toward the center of the basin. Beyond the faint scarp a system of valleys radiates outward for about 1000 km (Figure 9.10). These valleys may be fault troughs or chains of large coalescing secondary craters formed from strings of basin

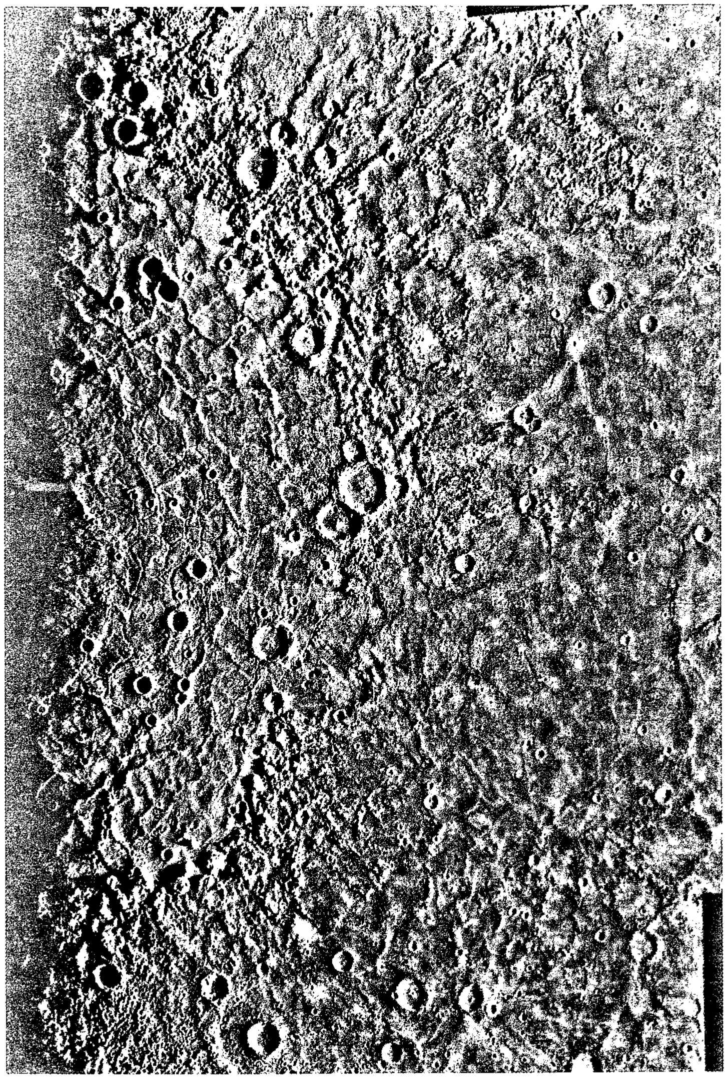

Figure 9.8. Photomosaic of the 1300 km diameter Caloris basin. This is the largest best preserved basin observed by *Mariner 10*.

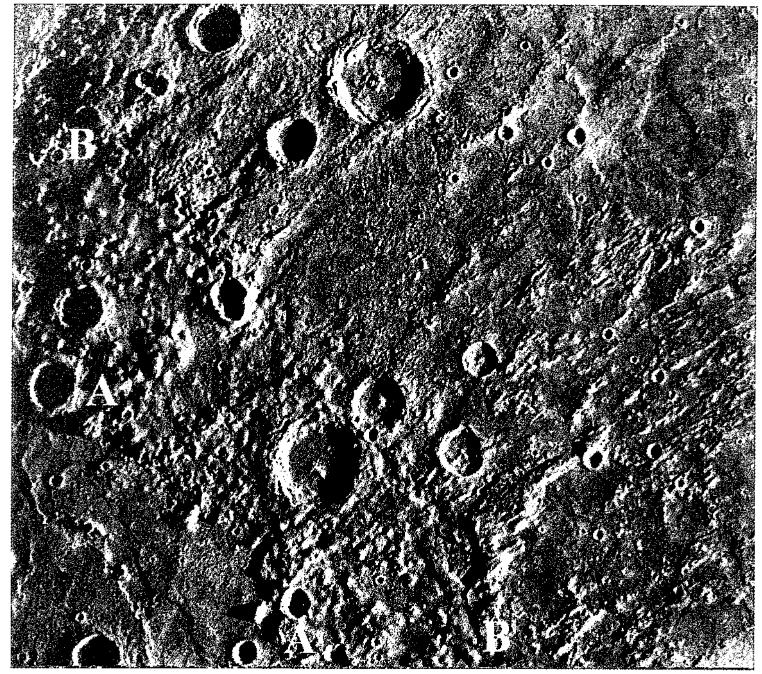

Figure 9.9. This detail of the Caloris basin's northeastern rim shows the main ring located at A–A and a weaker outer ring at B–B.

ejecta. Numerous crater clusters and irregular troughs are probably secondary craters. Some of these secondaries are over 20 km in diameter.

Beyond the basin rims are several areas of hummocky plains with numerous small hills that extend outward for several hundred km. This material is probably a combination of continuous ejecta including large fragments and a significant amount of impact melt (Figure 9.11). Surrounding these ejecta deposits are smooth plains that occur up to 2500 km from Caloris. These plains are probably volcanic deposits. They are discussed in Chapter 10.

The Caloris basin floor displays a structural pattern that is unique in the Solar System. The basin interior is filled with smooth plains that are highly fractured and ridged (Figures 9.12 and 9.13). The ridges form a pattern that is both concentric and radial to the basin center. They are similar in morphology to the Moon's mare ridges. However, in the Caloris basin they are much more numerous and have a radial component not seen on the Moon. The ridges are probably caused by

Figure 9.10. Linear valleys and ridges radiate from the rim of the Caloris basin. They were probably formed by ejecta from the impact basin.

compressive stresses as they are on the Moon. The ridges are transected by a system of younger tension fractures that also have a concentric and radial pattern (Figure 9.14). The fractures are up to 10 km wide and progressively increase in width and depth toward the basin's center (Figure 9.12). At the margin of the floor the fractures become very weak and completely disappear near the rim.

Vertical movements may account for both of these very different structures. Transection relationships indicate that the ridges formed first. They were probably caused by compressive stresses as the floor subsided. The floor covers about 30 degrees of latitude, and, therefore, has a substantial outward curvature. As a result the subsiding floor was compressed into a smaller area causing the ridges. The tensional fractures were formed next, possibly by vertical uplift that stretched the floor. Except at the Caloris antipode these tensional fractures are the only sign of tensional stresses on Mercury, making its tectonic history unique. The vertical movements may have been caused by subsidence due to the weight of crater

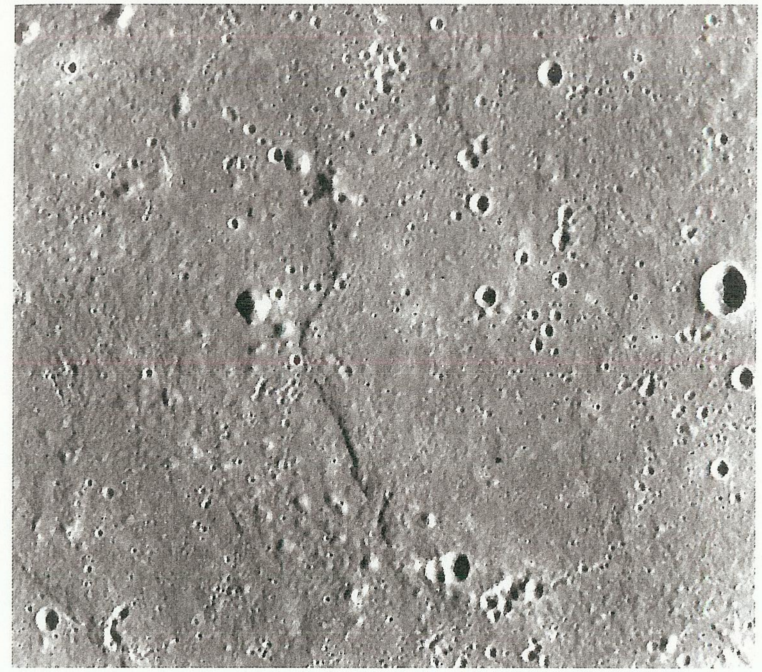

Figure 9.11. These rough plains with interbedded hills outside but near the Caloris basin are probably a continuous ejecta deposit of breccia and melt from the Caloris impact.

interior fill (lavas) as on the Moon. Uplift caused by upward migration of subsurface magmas may have caused the tensional stresses that formed the fractures.

9.6 HILLY AND LINEATED TERRAIN

As mentioned in Section 9.5, the Caloris basin-forming impact is also responsible for another type of terrain in a completely different part of Mercury. Directly opposite the center of the Caloris basin on the other side of the planet (the antipode) is located a peculiar, severely disrupted surface known as the hilly and lineated terrain. It covers an area seen in Mariner 10 images of at least 360,000 km^2. It probably extends further. It consists of hills, depressions, and valleys that disrupt pre-existing landforms. The hills are 5 to 10 km wide and up to 2 km high. Valleys are up to 15 km wide and over 120 km long. They form a roughly orthogonal pattern trending northeast and northwest. Crater rims have been disrupted in many cases,

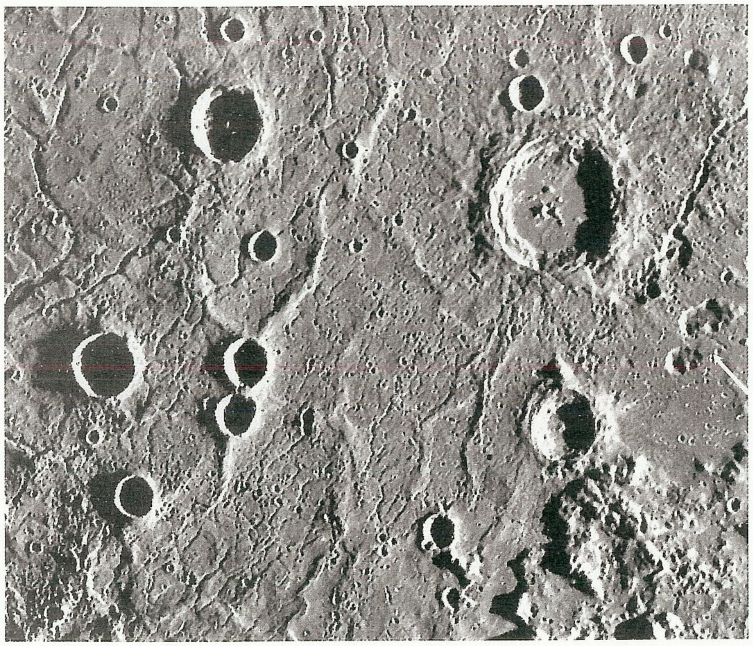

Figure 9.12. This image shows the ridged and fractured floor of the Caloris basin. The fractures transect the ridges and are therefore, younger. The irregular rimless depressions at the middle far right of the image (arrow) are probably volcanic collapse depressions. A relatively large abundance of potassium in Mercury's exosphere has been observed over the Caloris basin. It may be related to lavas from volcanic vents in turn related to the volcanic collapse depressions.

but their floors have been filled with younger plains. This indicates that volcanic activity occurred after the disrupting event (Figures 9.15, 9.16 and 9.17).

The hilly and lineated terrain is similar, but much larger in extent, to disrupted surfaces at the antipodal points of the Imbrium and Orientale basins on the Moon. The fact that these terrains occur at the antipodal points of large impact basins strongly suggests that they are the result of the impacts. Seismic waves generated by these impacts converge or focus at the antipodal regions (see Figure 9.18). Computer simulations of seismic wave propagation for impacts of this size show that the seismic effects in the antipodal regions can be enormous. The ground may experience vertical motions greater than 1 km in a matter of minutes, and tension fractures rend the crust to depths of tens of kilometers. This stress breaks the surface into a jumble of blocks and depressions like the hilly and lineated terrain. Models

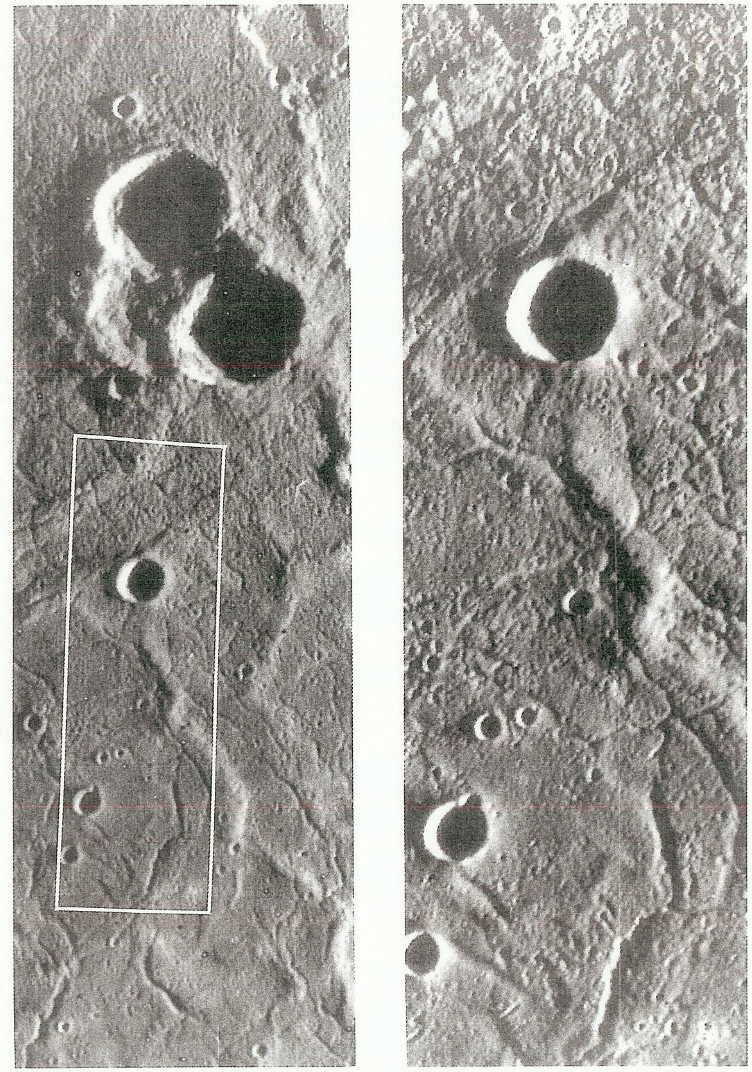

Figure 9.13. These third-encounter images show a small portion of the Caloris basin floor. The rectangle in the image on the left indicates the location of the image on the right.

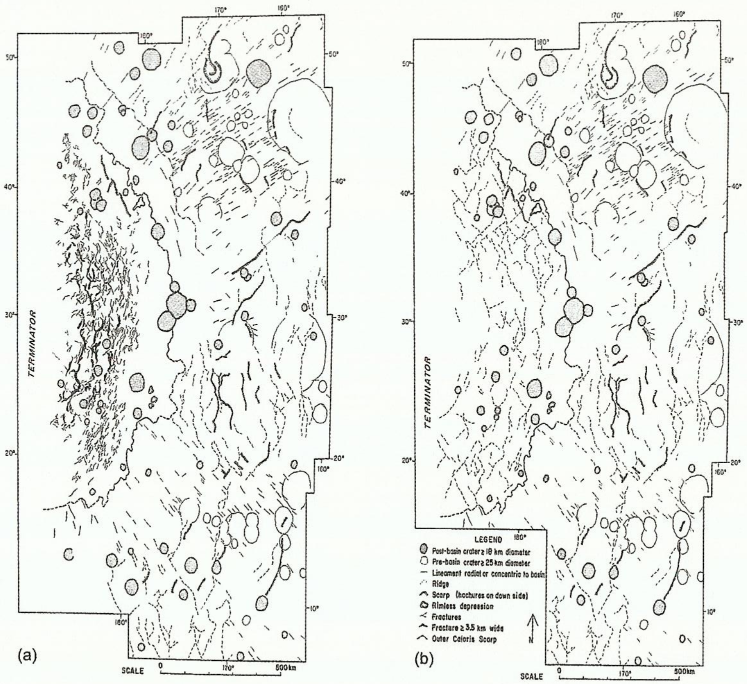

Figure 9.14. These maps show the pattern of fractures (a) and ridges (b) on the Caloris basin floor. Both systems show a radial and concentric component (from Strom, Trask, and Guest, 1975).

show the effects are enhanced by seismic waves refracted by Mercury's enormous iron core. This explains why the hilly and lineated terrain is much more extensive on Mercury than the Moon. Furthermore, fractures penetrating to great depth could provide egress to the surface for lavas that appear to have flooded the low lying areas within craters after their disruption. As at Caloris, enhanced potassium in Mercury's exosphere has been observed over the antipodal hilly and lineated terrain. It may be coming from the rocks formed from the lavas or from tension fractures.

9.7 ORIGIN OF IMPACTING BODIES

9.7.1 Asteroids

The origin of the objects responsible for the cratering record in the inner Solar System is somewhat controversial. Today the only objects that cross the inner

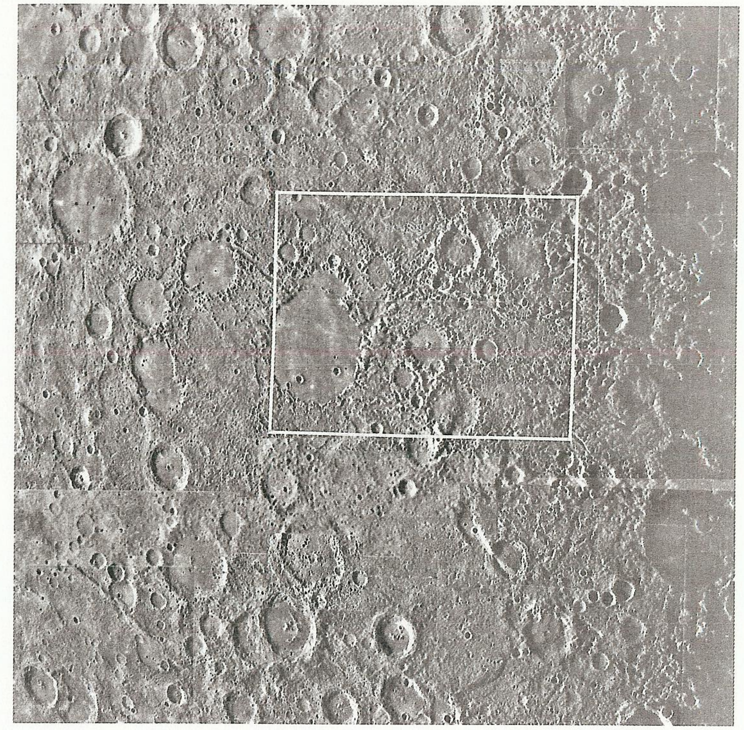

Figure 9.15. This photomosaic shows the region of Mercury's hilly and lineated terrain. The outlined area is the location of the higher resolution image shown in Figure 9.16.

planet orbits are comets and high eccentricity asteroids called Amors and Apollos. There is no doubt that they have, and still are, contributing to the cratering record. But are they the only source?

9.7.2 Elusive vulcanoids

Some people have speculated that there is a population of vulcanoids, or rocky bodies orbiting around the Sun closer to the Sun than Mercury. Perturbations on the Vulcanoids could cause impacts with the surface of Mercury. Recent searches have not found any, and it is likely that they do not exist.

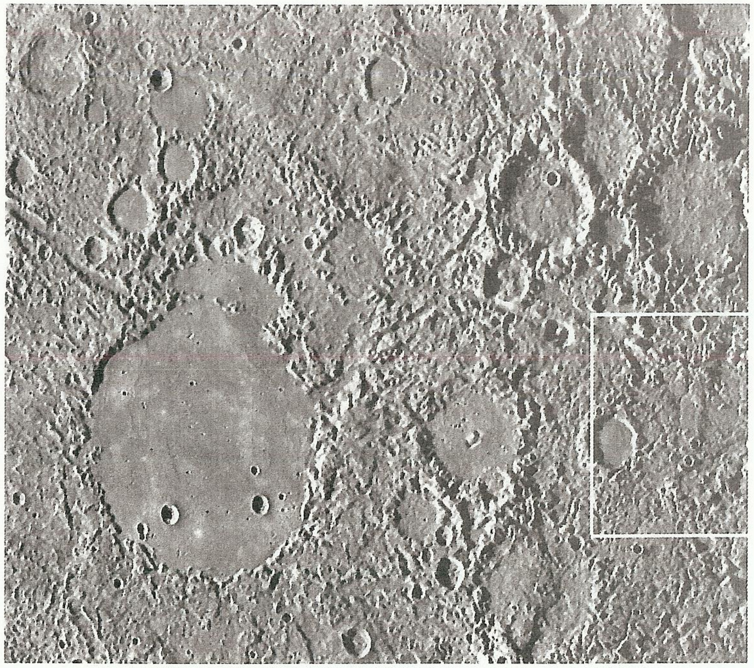

Figure 9.16. This image shows more detail of the hilly and lineated terrain. The smooth plains filling the large crater at left are younger than the hilly and lineated terrain. The outlined area can be seen at high-resolution in Figure 9.17.

9.7.3 Evidence for two collisional populations

Comparisons of the Solar System cratering record and dating of returned lunar rocks, including lunar meteorites, have provided some information on the origin of impactors. The manned *Apollo* missions to the Moon returned rocks from a variety of locations. From these samples it was learned that the relatively sparsely cratered mare lavas date from about 3.9 to 3.0 billion years old. The heavily cratered highlands are even older, dating from about 4.4 to 4.0 billion years. The lunar highlands accumulated their great abundance of craters, including the large mare-filled basins, over a geologically short time span of no more than 400 million years. On the other hand, the younger lunar maria accumulated their much smaller number of craters over the enormous span of 3 to 4 billion years (about 10 times longer than the luner highlands). This must mean that the Moon experienced a period of intense bombardment that ended early in its history about 3.9 billion years ago. It was

Figure 9.17. This is one of the highest resolution images of the hilly and lineated terrain taken by *Mariner 10*. It shows a broken-up surface of hills and valleys. The hills range from 0.1 to 1.8 km high. The large crater on the left is 31 km in diameter.

during this intense period of bombardment that most basins were formed. Since that period ended, large impacts have been relatively infrequent and no large basin-forming events have occurred.

There is some evidence that the period of heavy bombardment was a catastrophic event rather than a rapidly declining high flux of objects. Impact melts from 3 to possibly 6 impact basins indicate they were formed between 3.88 and 4.05 billion years ago. Furthermore, additional analyses of *Apollo* samples indicate the U-Pb and Rb-Sr systems were disturbed ~3.9 billion years ago. Recently analysed lunar meteorites also have impact melt that dates from about 3.9 billions years ago. These data suggest there was a catastrophic bombardment about 3.9 billion years ago that not only affected the Moon, but almost surely affected all the inner planets, including Mercury. Analyses of lunar impact melts indicate that at least one of these projectiles had a differentiated iron-rich core. Meteorite analyses

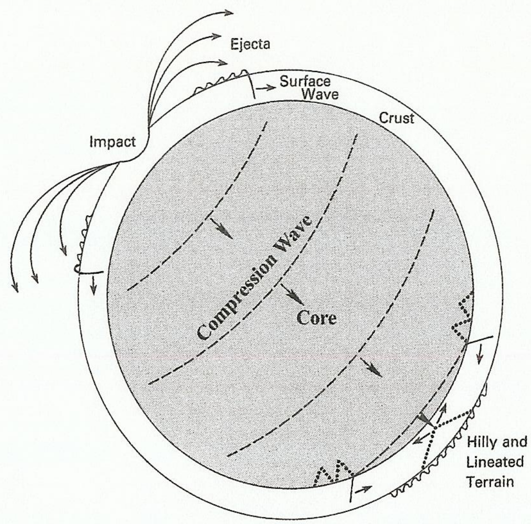

Figure 9.18. This diagram shows the probable cause of the hilly and lineated terrain. Seismic waves generated by the Caloris impact were focused at the antipodal point, causing large vertical ground movements resulting in the hilly and lineated terrain (courtesy Peter Schultz, Brown University).

indicate that the asteroids were also heavily cratered about 3.9 billion years ago. These data suggest the origin of the objects was the asteroid belt.

The impact crater size distributions for Mercury and other inner Solar System objects seem to be consistent with an early cataclysmic heavy bombardment. Crater size/frequency distributions measure the number of craters within certain size ranges. This in turn is a measure of the size distribution of the impacting objects when proper scaling relationships are taken into consideration. Crater abundances derived from size/frequency distributions are also used to date surfaces relative to each other, and also on an absolute time scale if the crater production rate is known.

The crater size/frequency distribution is conveniently displayed on what is called a "Relative" (R) plot. This type of plot was devised to better show the size distribution of craters, and the crater number densities for determining relative ages. On an R plot the size/frequency distribution is normalized to a differential -3 distribution function, or slope. The reason a -3 reference distribution is used is because most impact crater size/frequency distributions are within ± 1 of a -3 distribution. On an R plot a differential -3 distribution plots as a horizontal straight line. The vertical position of the line is a measure of the crater density or relative age; the higher the

Table 9.1. Size/frequency distributions for slopes of -2, -3, and -4.

	Slope		
Crater diameter (km)	-2	-3	-4
64	1	1	1
32	4	8	16
16	16	64	256
8	64	512	4096
4	256	4096	65536

vertical position, the higher the crater density and the older the surface. On an R plot a line sloping to the left at an angle of 45° is a differential -2 distribution, and one sloping to the right at 45° is a differential -4 distribution. Usually the data are binned into $\sqrt{2}$ increments because there are many more craters at small diameters than large diameters. For example, a distribution with slope -3 would have 1 crater of diameter 64 km, $(1/2)^{-3}$ craters (8) of 32 km diameter, $8 \times (1/2)^{-3}$ craters (64) of 16 km diameter, and $64 \times (1/2)^{-3}$ craters (512) of 8 km and so on. This is displayed in Table 9.1 along with size/frequency distributions for slopes of -2 and -4. Figure 9.19 is a diagramatic representation of the difference between a -3 and a -2 slope.

Mathematically, the R value is expressed as follows:

$$R = \frac{D^3 N}{A(b_u - b_l)},$$

where D is the geometric mean diameter of the size bin, N is the number of craters in the size bin, A is the area counted, b_u is the upper limit of the size bin, and b_l is the lower limit.

The heavily cratered surfaces of the Moon, Mars, and Mercury represent the period of heavy bombardment early Solar System history. These surfaces on Mercury, the Moon, and Mars all have similar crater distributions (Figure 9.20). They show a complex curve with about a -2 distribution at diameters less than about 50 km, a -3 distribution between 50 and 100 km, and about a -4 distribution between 100 and 500 km. At diameters greater than 500 km the statistics are too poor to determine a crater distribution with any confidence. One notable difference between the curve for the Moon and those for Mercury and Mars is that at diameters less than about 50 km there is a marked deficit of craters on Mercury and Mars compared to the Moon. This is almost surely due to the emplacement of intercrater plains material on Mercury and Mars compared to the Moon where these plains are extremely rare (see Figure 9.21). This strongly suggests that intercrater plains formation on Mercury was occurring during the period of heavy bombardment. The youngest smooth plains surfaces that surround and fill the Caloris basin also show a similar crater size/frequency distribution as the

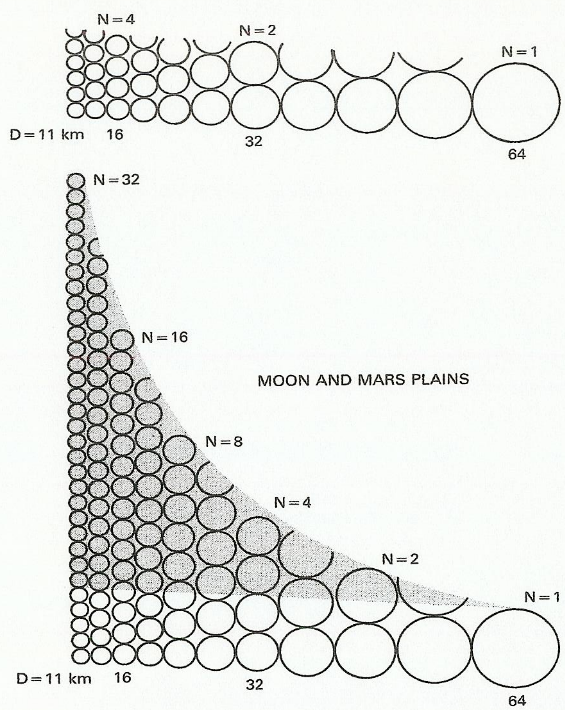

Figure 9.19. This diagram illustrates the difference between the size/frequency distributions of craters between 11 and 64 km in diameter found on the terrestrial planets. The size distribution in the upper diagram represents the heavily cratered highlands of the Moon that resulted from the period of heavy bombardment. It has a differential −2 slope. Somewhat similar distributions occur in the heavily cratered terrain on Mars and Mercury but the slopes are more like a −1.5 differential slope. The size distribution in the lower diagram represents the lightly cratered plains on the Moon and Mars. It has a differential −3 slope. The shaded area indicates the difference between the two crater populations. (See text for explanation.)

highland, but at a lower density (Figure 9.20). The crater density on these younger surfaces is much greater than on the lunar maria.The post-Caloris curve is similar to that of Mercury's highlands but it is shallower because it has not been effected by plains emplacement. It is at a lower level because the post Caloris surface is younger than the highlands, and its shape indicates that it is part of the period of heavy bomardment (probably near the end of that period).

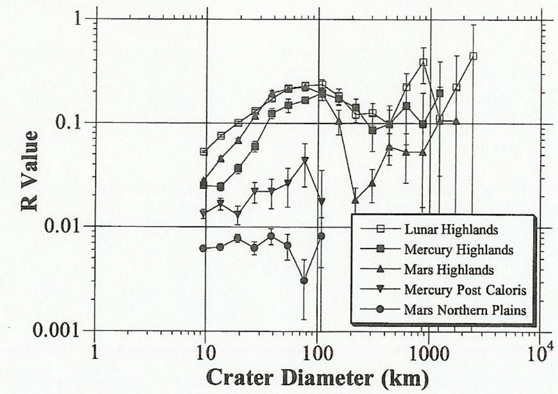

Figure 9.20. This R plot is a comparison of the crater size/frequency distribution of the lunar, Mercurian, and Martian heavily cratered highlands. They all have a similar shape indicating a common origin. The steeper slopes for Mercury and Mars at smaller diameters are the result of obliteration of craters by intercrater plains formation. Also shown is the size distribution of the post-Caloris crater population and the lightly cratered relatively young surfaces on Mars (see text for explanation).

A comparison of the *R* plots of the highland cratering records on Mercury, the Moon and Mars describes the nature of the objects that were impacting during the period of heavy bombardment within the inner solar system. The curves all have similar shapes except at diameters less than about 40 km where intercrater plains emplacement has modified the curves for Mercury and Mars as mentioned above. However, at diameters between about 40 km and 150 km, where the curves are probably unaffected by plains emplacement, the curves are laterally displaced with respect to each other. In fact, they are displaced in a manner that requires high velocities for planets at smaller heliocentric distances; larger craters on Mercury and smaller craters on Mars compared to a given size crater on the Moon. The best fit of the curves shows that for a 100 km diameter crater on the Moon, the crater size is 120 km diameter on Mercury and 80 km diameter on Mars. A comparison of the ratios of impact velocities derived from scaling laws and their required eccentricities suggest that the objects responsible for the period of heavy bombardment were confined to the inner solar system with semimajor axes between about 0.8 and 1.2 AU (Figures 9.22 and 9.23).

9.7.4 Surfaces younger than the period of heavy bombardment

Mercury may have some surfaces younger than the period of heavy bombardment on the unimaged portion of the planet. We will have to await further exploration to answer that question.

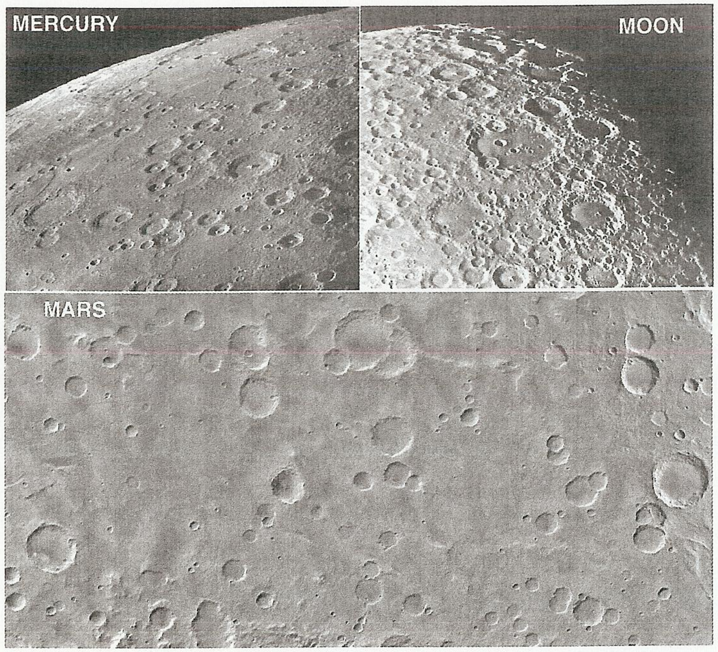

Figure 9.21. This composite image shows extensive intercrater plains in the heavily cratered highlands of Mercury (upper left) and Mars (bottom), but little or no intercrater plains on the Moon (upper right). The implacement of intercrater plains on Mars and Mercury probably resulted in the greater paucity of craters at diameters less then about 40 km compared to the Moon. The individual images are not to scale.

Young surfaces on the Moon and Mars have a significantly different size/frequency distribution. They show a −3 distribution in the diameter range of about 1 to 100 km. There are very few craters larger than 100 km on these young surfaces (see Figure 9.20). At least on Mars, and probably on the Moon, this population of craters is most likely the result of impacts from the *collisionally evolved* asteroid belt.

Since the objects responsible for the period of heavy bombardment have a different size/frequency distribution, they appear to come from a different population, but one confined to the inner Solar System. One possibility is they were primordial, *collisionally unevolved* asteroids that were dynamically ejected from the asteroid belt by the combined gravitational perturbations of Jupiter and planetary embryos retained from the formation of the inner planets. Another possibility is that

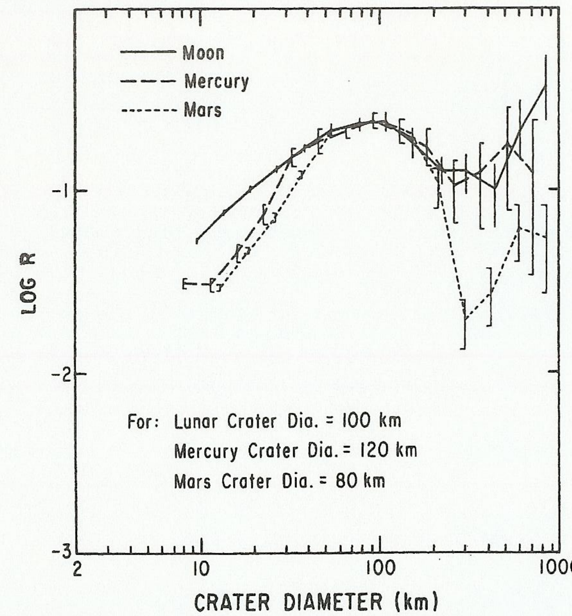

Figure 9.22. The crater size/frequency distributions for the highlands of the Moon, Mars, and Mercury (Figure 9.20) have been matched from about 40 km to 150 km diameter (the range not effected by intercrater plains emplacement and having good statistics). The lateral shifts in the curves require higher planet impact velocities with decreasing heliocentric distance; larger craters on Mercury and smaller ones on Mars compared to a given size crater on the Moon (from Strom and Neukum, 1988).

they could be fragments from a giant collision in the asteroid belt very early in its history. Either of these origins could provide a cataclysmic bombardment of the inner planets. However, there may by other ways to produce this ancient population of objects.

9.8 RELATIVE AND ABSOLUTE AGES

The crater abundance superposed on various geologic units can be used to determine the age of a surface relative to other geologic units. This technique, together with embayment relationships among units and transection relationships between tectonic structures and various units, forms the basis for determining the order of

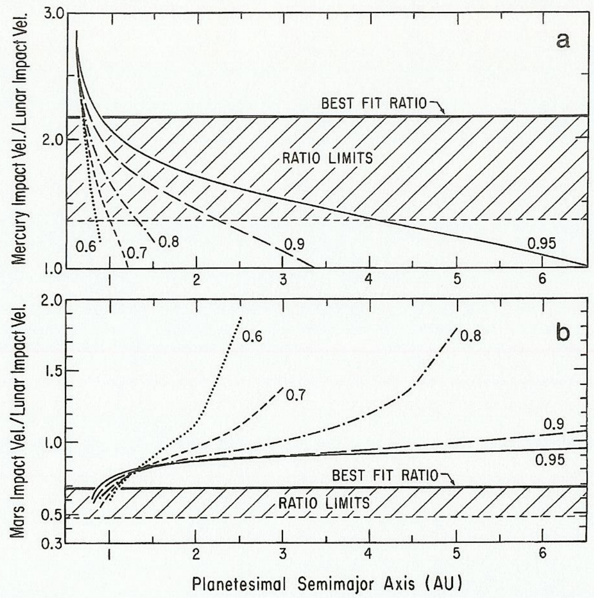

Figure 9.23. Plot of the impact velocity ratios Mercury/Moon (a) and Mars/Moon (b) derived from matching the highlands crater curves (Figure 9.22), verses impactor semimajor axes for eccentricities from 0.6 to 0.95. The hatched areas are the limiting impact velocity ratios for an acceptable curve fit, while the solid horizontal lines are the ratios derived from the best curve fit shown in Figure 9.22. Only planetesimals with semimajor axes between about 0.8 and 1.2 AU lie within the same region of the impact velocity ratio limits. Jupiter crossers (objects that cross the orbit of Jupiter) have semimajor axes greater than 2.7 AU (from Strom and Neukum, 1988).

emplacement (the relative age) of geologic units. The geologic maps of Mercury are based on these techniques. The age of a surface based on the cratering record requires that the surface is: (1) not saturated with craters (i.e., it is a *production crater population*), (2) that only superposed craters are counted (no relic or ghost craters from an underling unit); and (3) that all secondary and volcanic craters are eliminated from the counts.

If one knows the rate at which craters are formed, then the age of the surface can be determined. The rate of crater formation depends on a knowledge of the rate at which various objects collide with the planet or satellite. This, in turn, depends on the origin of the impacting objects, and the proportion of each type of impactor (e.g., comet or asteroid, that has impacted the planet). Obviously, estimates of these factors contain large uncertainties and, therefore, the estimated

absolute ages are uncertain. However, on the Moon, where surfaces have been dated from returned samples, it has been possible to date surfaces by comparing the crater abundances on surfaces of known absolute ages to derive a crater production function that can be used to measure the ages of other surfaces where no rocks have been returned. This works quite well on the Moon, but extrapolating this crater production rate to other planets can result in significant errors. One must first assume that the impacting objects were the same at the Moon and the planet, and then scale the production function by certain scaling laws. However, we know that the terrestrial planets have been impacted by at least two populations of objects, comets and asteroids. If the period of heavy bombardment was the result of a catastrophic event then a third population may be involved. Furthermore, there are two crater populations in the inner solar system, one for younger surfaces and another for ancient surfaces. Any extrapolations must use the correct crater population at both bodies. In the outer Solar System the problem is even more complex and extremely uncertain.

9.8.1 Mercury's surface is ancient

On Mercury, absolute ages are derived from those determined for the Moon. The dependence of the Mercurian cratering rate is assumed to be the same as for the Moon. Also considerations of asteroid and comet impact probabilities at Mercury, and corrections for impact velocities, scaling, and gravitational focusing effects are taken into account. It is obvious that there can be relatively large errors in the age determinations. However, it is not as bad as it seems. The period of heavy bombardment almost surely ended on Mercury at the same time it ended on the Moon; before about 3.8 billion years ago. Therefore, surfaces that show a crater population associated with the period of heavy bombardment must be $\geq$3.8 billion years. Since all surfaces on Mercury explored to date show this crater population, they are probably between 3.8 and 4.5 billion years old. Surface ages derived for units with different crater densities are extrapolated between these extremes with the Caloris basin assumed to have formed 3.8 billion years ago.

9.8.2 Will there be younger terrains on the unimaged side?

One must be very cautious because we have only seen 45% of the surface and only about 25% of the surface was viewed at sun angles suitable for terrain analysis. Other areas of Mercury could be considerably younger than those where crater counts are currently available.